Journal of Marine Research, 69, 523–543, 2011

Ocean stratification under oscillatory surface buoyancy forcing

by Ross W. Griffiths[1,2], Nicola Maher[1] and Graham O. Hughes[1]

ABSTRACT

Laboratory experiments with overturning circulation driven by oscillatory heat fluxes at one boundary are used to explore implications, for the ocean stratification, of a cyclic fluctuation in sea-surface buoyancy forcing. Fluctuations having a range of periods spanning the timescale for global recycling of the ocean volume through the thermocline are considered, with emphasis on inter-hemispheric 'see-saw' oscillations. Episodic sinking of dense water in the oceans is represented by convection in a channel with a base that is cooled over a central region and subjected to oscillatory heating near both ends, while providing a constant total heat input. For this simplified system the time-average interior temperature is found to be insensitive to the forcing period, but does vary with oscillation amplitude, whereas the interior fluctuations increase with forcing period. The circulation and density field are significantly different from those given by a steady forcing equal to the time-average of the actual oscillatory forcing, even for high-frequency oscillations. The results indicate that the overall stratification lies between that expected from the strongest phase of deep sinking and that given by symmetric sinking in both hemispheres. Glacial cycles are predicted to involve significant temperature fluctuations in the abyssal ocean. However, they are too short for the ocean to remain in quasi-equilibrium with the changing boundary conditions.

1. Introduction

Thermal and wind stress boundary conditions at the sea surface are not steady and involve global scale fluctuations ranging from the seasonal 'see-saw' forcing between hemispheres to climate fluctuations on millennial and longer timescales. This raises the questions: how do the circulation and stratification of the oceans respond to different external forcing timescales and to what extent do they adjust to changing surface boundary conditions? Earth's seasonal cycle is clearly too short for the deep ocean stratification to adjust substantially within each season. The glacial climate cycles of order 100,000 years might, however, be long enough for the ocean circulation to remain close to equilibrium with its boundary conditions. As a simple illustration of the way in which the stratification can respond, Killworth and Turner (1982) examined a turbulent plume falling from a source of

1. Research School of Earth Sciences, Australian National University, Canberra, ACT 0200, Australia.
2. Corresponding author. ***email: ross.griffiths@anu.edu.au***

unstable buoyancy that oscillated in strength. This produced a 'filling-box' density stratification that is set by the largest buoyancy flux of the source rather than by the mean flux. An implication is that the annual mean ocean circulation is not the same as that generated by a steady forcing equal to the annual mean forcing. However, the oscillating plume experiment did not have a zero net buoyancy input over a cycle, as is expected for the global ocean, and the role of the oscillation period was not explored. Naturally wind stress variations also influence the ocean circulation, and potentially the density stratification. However it is of use to understand the response under buoyancy forcing alone. Here we investigate, in a simple laboratory model, the response to an oscillatory buoyancy forcing applied at the surface with zero net buoyancy input over the long term.

A range of ocean general circulation models have addressed a meridional overturning circulation forced by surface buoyancy fluxes (Bryan, 1987; Colin de Verdière, 1988; Suginohara and Aoki, 1991; Wright and Stocker, 1991; Park and Bryan, 2001; Rahmstorf, 1996). Despite their inherent difficulties in resolving convection, dense slope currents and mixing, the computed solutions are in general agreement with the the magnitude of the ocean overturning inferred from ocean measurements. Simple mathematical models (Hughes and Griffiths, 2006; Hughes *et al.*, 2007) show explicitly how broadly dispersed upward advection of water in the ocean interior (assuming a Munk-like advection-diffusion balance there - Munk (1966)) can be coupled with localized, dense, turbulent plumes or overflows at high latitudes to find a closed solution, again predicting overturning comparable to that observed. Turbulent entrainment into the dense plumes is indicated to play a substantial global role. Convective overturning forced by steady surface buoyancy fluxes, termed horizontal convection, has also been examined through laboratory experiments (Rossby, 1965; Hignett *et al.*, 1981; Mullarney *et al.*, 2004; Wang and Huang, 2005) and complementary numerical convection simulations (Beardsley and Festa, 1972; Rossby, 1998; Mullarney *et al.*, 2004, 2006; Hughes and Griffiths, 2008). In recent experiments with a long box heated through two regions towards the ends of the base and cooled through the central half of the base (Coman *et al.*, 2010), the circulation was shown to be sensitive to the ratio of heat inputs at the two heated regions. In particular the heating ratio determined the relative strengths and depths of penetration of the two end wall plumes.

In an equilibrated circulation with steady surface forcing there must be zero net heat transport through any level (Paparella and Young, 2002). The same condition applies to the heat transport averaged over a large number of cycles in flow driven by a fluctuating forcing. However, changing boundary conditions will lead to time-dependent convection (Rossby, 1998) and the somewhat delicate balance that characterizes circulation under steady boundary conditions will not be attained. In general, oscillatory boundary conditions can give a net vertical flux of buoyancy that is sustained over a substantial fraction of a cycle. Hence the time-dependent flow will involve, periodically, a much stronger overturning. Most previous studies of horizontal convection forced by differential surface buoyancy conditions have involved a single region of destabilizing buoyancy flux. In that case an oscillatory flux is expected to give rise to a periodic "shut-down" of deep sinking, during which, circulation

is limited to a shallower layer (Manabe and Stouffer, 1995). We expect also that the flow behavior will depend on the period of the oscillatory forcing relative to internal response timescales, such as the time required for a recycling of the volume of the domain through the boundary layer and adjustment to new boundary conditions. It is not clear that we can apply the Killworth and Turner (1982) results for a turbulent plume of oscillatory source strength, given the net buoyancy input in that case.

In this paper we examine the unsteady convection problem with two spatially separated destabilizing regions between which there is a 'see-saw' oscillation of the thermal forcing. We choose the special case of a constant total heat input in order to minimize the number of variables, and also for its geophysical relevance. The experiments focus on the stratification in the overturning circulation and the role of turbulent plumes (or the dense overflows and slope currents in the oceans). The dependence of the stratification and interior temperature on the external forcing period and amplitude are measured for this idealized case. We comment on the likely effects of various external forcing timescales on the abyssal ocean density.

2. Apparatus and methods

a. Apparatus

The experiments used a rectangular box that has been described in detail elsewhere (Coman *et al.*, 2010) along with a description of circulation under steady thermal forcing from the horizontal base, with two heated regions separated by a cooled region. The internal dimensions were: length $L = 1.25$ m, height $D = 200$ mm and width 150 mm. The box had double-glazed side walls with argon gas in the 18 mm gap, 19 mm thick acrylic inner side and end walls, a triple-glazed acrylic lid (a unit 75-mm thick surrounded by the side walls and including two gaps filled with argon). All surfaces were further insulated by 100 mm of expanded polystyrene foam. The base was a single copper plate 10-mm thick surrounded by the side walls. The working fluid was de-aerated, filtered water with a small amount of domestic bleach to inhibit biological growth.

Heat was removed from the box by a heat exchanger that brought coolant, pumped from a constant temperature bath, into direct contact with the copper base. This cooled region was 600-mm long and centered on the mid-point of the box (Fig. 1). The coolant bath was held at 16 ± 0.02°C. Heat was provided by two electrical resistance mats (each 300-mm long and 150-mm wide) clamped beneath the left and right end quarters of the base. A 25-mm insulator separated each heating mat from the cooling region. Beneath each heating element was 40 mm of high temperature insulation and the entire assembly sat on 100 mm of expanded foam board. Each heating mat produced a heat flux uniformly over its area. Purpose-designed microprocessor-controlled power supplies delivered a specified total power to each heating mat to ± 0.05 W. The controllers were programmed to vary the power input as desired. The inner surface of the copper base was level to within 1 in 1000. The room temperature was 27 ± 1°C.

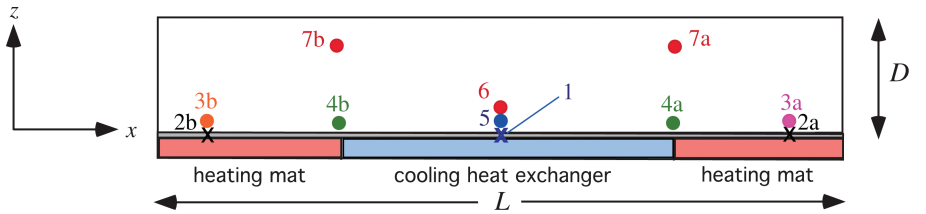

Figure 1. Side view of the heating and cooling arrangement showing thermistor locations (dots): 8 in the flow and 3 in the base of the tank. Thermistors labeled 3a,b, 4a,b and 5 were also used to take vertical profiles through the depth. Thermistor numbers and colors are keyed to data in Figures 2, 4 and 5.

Simple flow visualizations and video movies of the flow were obtained by slowly releasing neutrally buoyant dye solution from a 1-mm diameter tube into the stable boundary layer near each end of the cooled section of the base. From there the dye was advected in the boundary layer, mixed vertically within a convectively unstable lower portion of the boundary layer above each heated region, and carried upward in the end wall plumes. Attempts to use Particle Image Velocimetry in similar experiments failed as a result of sedimentation of particles during the long period required for thermal equilibrium, which left either insufficient suspended particles or slowly changing thermal boundary conditions where the particles accumulated on the base.

Temperatures in the flow were measured using a set of eight fast-response thermistors. In order to facilitate vertical profiling the thermistors were supported through small holes in the lid and fixed to a single computer-controlled traversing mechanism. Thermistors were held stationary for temperature-time records (at positions along the bottom boundary layer $z/D = 0.025$ and $x/L = 0.08, 0.24, 0.5, 0.72, 0.92$; near the top of the boundary layer $z/D = 0.15$, $x/L = 0.5$; and high in the box $z/D = 0.85$, $x/L = 0.24, 0.72$; all close to the centre line of the box: Fig. 1). The time records were occasionally interrupted to measure vertical profiles with the lower five thermistors. An additional three thermistors were embedded in the copper base, along the centre line at locations $x/L = 0.08, 0.92$ (in the heated regions) and $x/L = 0.5$ (the centre of the cooled region).

b. Procedure

Each heating controller was first set to supply constant powers $H_1 = H_2 = 140.0\,\mathrm{W}$ (giving a flux $F = 3111\,\mathrm{Wm}^{-2}$). The approach to thermal equilibrium was monitored using a time record of the temperatures logged at 10 Hz; windowed averages were recorded at 10 s intervals. Equilibration required several days (Fig. 2) and was judged to have been reached after the interior temperatures had been stationary to within $\pm 0.01°\mathrm{C}$ for at least one day. In this equilibrium state the steady power input was matched by the time-averaged rate of cooling through the central region of the base (plus a small heat loss to the room). An interesting observation was a substantially greater amplitude of variability, at relatively

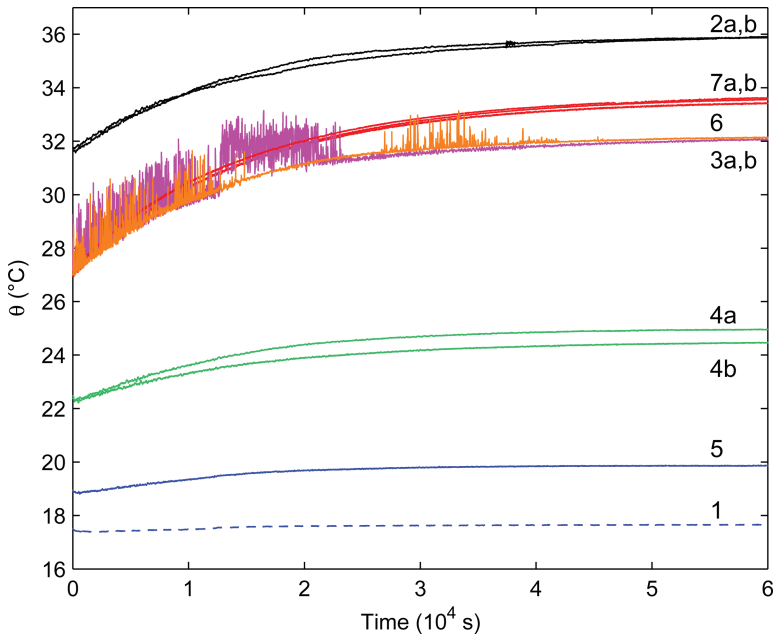

Figure 2. Adjustment to equilibrium in the case of steady symmetric heating (Run 0 in Table 1). Raw temperature records are plotted from eight locations in the flow and three in the base: in order of increasing temperatures (color coded and keyed to thermistor location numbers in Fig. 1); data are from the cooled base (1, broken blue line); the mid-point of the cold boundary layer (5, solid blue line); slightly higher in the boundary layer at each end of the cooled base region (4a,b, green), the heated boundary layer near each end of the box (3a,b, magenta and orange), three locations in the interior (6, 7a, 7b, red lines), and the heated base near each end (2a,b, black lines). Note the small-scale boundary layer convection (high frequency signals at 3a,b). The box was initially at 27°C but the cooling heat exchanger operated for a short time to cool the central region of the base before heating and measurements began. Fitting an exponential approach towards the final temperature for the interior (red lines) gives an e-folding equilibration time $\tau = 1.54 \times 10^4$ s.

high frequencies, in the heated parts of the bottom boundary layer (thermistors 3a,b) during the thermal adjustment. Consistent with this, dye tracer revealed that penetrative convection within the boundary layer was more vigorous and the consequent mixed layer (Mullarney *et al.*, 2004) was deeper during this period compared to the final stationary state. The greater instability follows the net buoyancy input to the box during the flow adjustment. More will be said about this aspect in Section 3, as it also occurs through much of the cycle of oscillatory forcing despite a zero net heat input at all times.

Measurements were taken for the equilibrium, symmetric steadily-forced control case. The same procedure was repeated for a second control case having the same total heat input, but with the full 280 W supplied to just one of the heated regions; this forcing represents the maximum asymmetry in the oscillatory forcing.

The programmed sinusoidal variation of the power inputs was always started after the system reached the stationary state with symmetric forcing. The two heat inputs then varied about a mean value of 140.0 W, with a period T_0 and frequency $\omega = 2\pi/T_0$. The two heat inputs were in all cases given equal oscillation amplitudes $140.0a$ (W), where $0 \leq a \leq 1$, but were 180° out of phase:

$$H_1 = 140[1 + a\sin(\omega t)],\ H_2 = 140[1 + a\sin(\omega t - \pi)]. \tag{1}$$

Both end regions were always heating (although the input power vanished momentarily in each cycle for the case $a = 1$) and the total heat input $H = H_1 + H_2 = 280$ W was always constant in time. Periods T_0 from 20 minutes to 19 hours were used. A number of steadily-forced cases with constant heating differences $(H_1 - H_2)/H$ were examined by Coman *et al.* (2010). The two steady cases $[H_1 = 280\,\mathrm{W}, H_2 = 0]$ and $[H_1 = H_2 = 140\,\mathrm{W}]$ were repeated here in order to assure accurate comparisons. The first of these represents the extreme, through which the oscillatory case $[a = 1, T_0 \to \infty]$ would pass periodically. The second comparison represents the case $a = 0$ (and given finite conductivity in the copper base, which damps rapid variations, this also represents the case $T_0 \to 0$).

c. Parameters

The flow is described by a Rayleigh number, Prandtl number, box aspect ratio, and the dimensionless amplitude and period of the forcing. As in the previous experiments with steady forcing (Mullarney *et al.*, 2004; Coman *et al.*, 2010), the flux Rayleigh number is defined by $Ra_F = g\alpha F L^4/\rho_0 c_p \nu\kappa^2$, where g is the gravitational acceleration, α is the thermal expansion coefficient, F is the time-averaged heat input per unit area in the heated regions (3111 Wm^{-2} in the present experiments), ρ_0 is a reference density of the water, c_p is the specific heat, ν is the viscosity, κ is the thermal diffusivity and L is the length of the box. We chose to define the Rayleigh number in terms of the length L rather than the depth D, as is the convention for horizontal convection in which the heat flux or temperature difference is applied over the length. The aspect ratio $A = L/H$ does not then appear in the Nusselt-Rayleigh number relation (Rossby, 1965). In the present experiments $A = 6.25$. All physical properties of water were evaluated at the measured temperature in the bulk of the box. The property most sensitive to temperature is the expansion coefficient, which for our interior temperatures between 33.1 and 35.5°C lies in the range $\alpha = (3.2 - 3.6) \times 10^{-4\circ}\mathrm{C}^{-1}$. In all cases $Ra_F = (3.21 - 3.66) \times 10^{14}$. The corresponding temperature-based Rayleigh number is $Ra = g\alpha\Delta\theta L^3/\nu\kappa = (1.2 - 1.3) \times 10^{12}$, where we define $\Delta\theta$ as a reference temperature difference - the maximum horizontal difference at the forcing boundary, as determined by the flow. The molecular diffusivity is effectively constant at $\kappa = 1.49 \times 10^{-7}\,\mathrm{m}^2\mathrm{s}^{-1}$ and the Prandtl number is nearly constant: $Pr = \nu/\kappa \approx 5.1$.

Under constant forcing the temperature difference $\Delta\theta$ is related to the heat flux F through the established relation

$$Nu = C Ra_F^{1/6}, \tag{2}$$

Table 1. Oscillation periods, amplitudes and water properties for each experiment. Two control cases with steady symmetric (run 0) and steady asymmetric (run 5) forcing are included. T_0 is the oscillation period, a is the dimensionless amplitude in equation (1), and $\Delta\theta$ is the normalising temperature difference calculated from the scaling analysis (Eq. 3). The differences in $\Delta\theta$ are entirely a result of the dependence of physical properties of water, and particularly the thermal expansion coefficient, on temperature. The time-averaged interior temperature, also averaged over three thermistors, is shown. All cases have a total heat input 280 ± 0.1 W.

Run	Period T_0 (*hrs*)	Amplitude (W)	Amplitude a	$\Delta\theta$ ($^\circ C$)	interior average $\bar{\theta}(^\circ C)$
0	steady	symmetric 140, 140	0	23.38	33.3
5	steady	asymmetric 280, 0	0	22.71	37.1
1	6.283	140	1	22.95	35.65
2	2.094	140	1	22.94	35.7
3	0.698	140	1	22.96	35.6
4	6.283	140	1	22.94	35.7
6	0.349	140	1	22.99	35.4
7	18.85	140	1	22.94	35.7
8	0.667	7	0.05	23.33	33.55
9	0.667	14	0.10	23.32	33.6
10	0.667	28	0.20	23.28	33.8

where the Nusselt number $Nu = FL/(\rho_0 c_p \kappa \Delta\theta)$. Hence

$$\Delta\theta = FL/\left(\rho_0 c_p \kappa C Ra_F^{1/6}\right) = C^{-1}(\nu/g\alpha)^{1/6}(\rho_0 c_p)^{-5/6}\kappa^{-2/3}L^{1/3}F^{5/6}. \qquad (3)$$

The numerical coefficient C has been evaluated for the case of a uniform imposed heat flux through one half of the base and a uniform imposed temperature for the other half (for the present value of Pr): from laboratory experiments $C \approx 0.82$ and from numerical solutions $C \approx 0.62$ (Mullarney *et al.*, 2004), whereas from a theoretical model $C \approx 0.75$ (Hughes *et al.*, 2007). Given that there was no externally prescribed temperature difference in the present experiments, the temperature difference (3) generated by steady forcing was used to normalize the measured temperature differences in the oscillatory cases, and we use the empirical coefficient $C = 0.82$.

A simple external timescale for the flow, beside the imposed oscillation period, is that for molecular diffusion of heat through the depth of the box: $D^2/\kappa \approx 2.7 \times 10^5$ s. We examined periods (Table 1) that spanned nearly two orders of magnitude, with the longest period being one quarter of the diffusion time. The thermal adjustment to steady forcing, as illustrated in Figure 2, was 99% complete within just one quarter of a diffusion time.

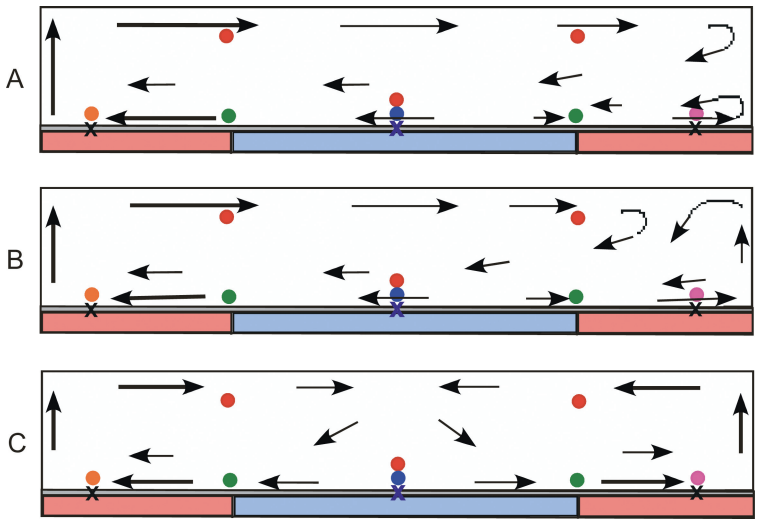

Figure 3. Sketches of the circulation patterns at three phases of the periodic oscillation, which are labeled A, B, C in Figure 5: A - when maximum heat input is applied at left; B - at 1/8th of a forcing period later when the weaker plume at left has penetrated to the top; C - a further 1/8th of a period later when there is equal power supplied to each end. One half period after 'A' (not shown) the flow is the same as at 'A' but mirrored about the mid-point of the box with the strong plume at the right hand end. Dots are thermistor locations as in Figure 1.

Conduction of heat through the base placed a lower limit, estimated at around 100 s, on achievable periods.

3. Results

The circulation was always unsteady (Mullarney *et al.*, 2004), including small-scale penetrative convection in the heated portions of the bottom boundary layer, shear instability in the upwelling plumes at the ends of the box, and large eddies in the plume outflows at the top of the box. Video movies of dye tracer in the flow also showed that the ascending plume at each end of the box oscillated in strength and penetration height. Given the difficulty of portraying this changing circulation pattern using still images of the dye tracer, we instead sketch the flow in Figure 3. The velocity fields were qualitatively similar to those in the related cases of asymmetric steady forcing, for which images of dye advection can be seen in Figures 2-4 of Coman *et al.* (2010). The plume at the more strongly heated end at any time was more vigorous and turbulent, and ascended to the top of the box (Fig. 3a). The plume at the other end at the same time ascended only part way: at its weakest phase it formed a return flow, or intrusion, immediately above the bottom boundary layer. As the heating imbalance reversed, the weaker plume grew stronger, until it penetrated to the top of the box (Fig. 3b) shortly before the two ends received equal input power. The plume outflows

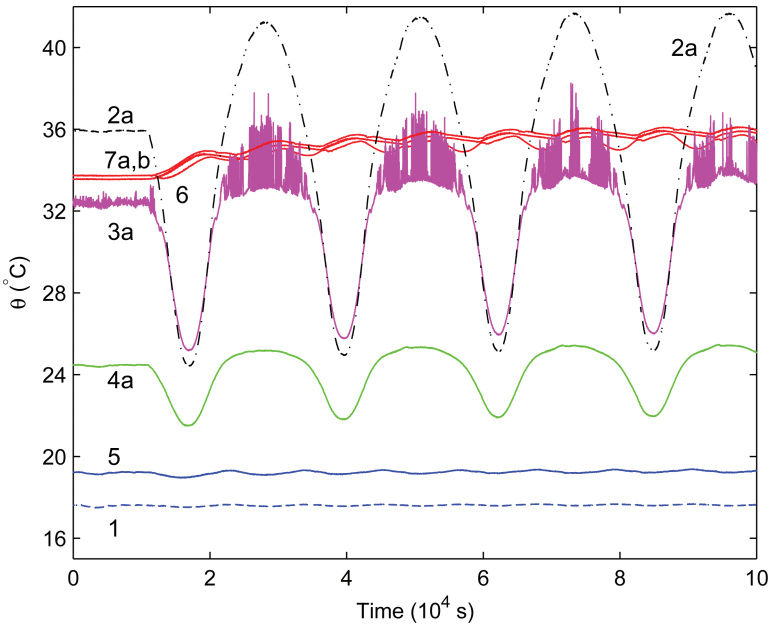

Figure 4. Temperatures during the adjustment from an initial steady forcing state (equal heat input to both heating regions) to a new large-time state with sinusoidal 'see-saw' forcing (Run 1 in Table 1, $T_0 = 6.28\,\text{hrs} = 2.26 \times 10^4\,\text{s}$, $a = 1$). Oscillatory forcing began at Time $= 1.1 \times 10^4$ s. For legibility, redundant data from the boundary layer on the left-hand end are omitted - they showed identical behavior 180° out of phase. Line colors and numbers are again keyed to the thermistor numbers in Figure 1. Base temperatures are broken lines, flow temperatures are solid lines. Note that an inner part of the bottom boundary layer is hotter than 3a during the stronger heating phase at that end, and supplies water to the plume that can rise to the top. The interior record (red) having the slightly larger fluctuation is from just above the boundary layer at the mid-point of the box (thermistor 6). Temperatures at large times were periodic at precisely the period of the applied heat flux.

along the top of the box similarly took turns at being the stronger, with the strongest phase of a plume driving an outflow along the full length of the box (Fig. 3a). In this phase the stronger plume outflow reached all the way to the opposite end wall even at the smallest forcing amplitude examined (consistent with the sensitivity to forcing asymmetry reported by Coman *et al.* (2010) in the case of steady forcing). When the base temperatures at the two ends were equal, twice in each cycle, the flow passed through a symmetric stage in which the confluence of the two plume outflows was halfway along the lid of the box (Fig. 3c). The weaker plume proceeded to become the stronger and the asymmetry of flow as sketched in Figure 3 reversed.

Temperature records reveal the flow behavior (Fig. 4). Immediately after the sinusoidal forcing started one heating mat received an increasing power input, the other a decreasing input (the temperature in only one end is plotted). The subsequent periodic fluctuation of

boundary and flow temperatures was initially superposed on a slower secular variation, until the new stationary state was approached in less than 10^5 s. Once in the long-time stationary state the interior flow far above the boundary layer experienced small, but significant fluctuations at half the period of the imposed oscillation. The cooled region of the base was successfully maintained at a constant temperature θ_c to within 0.2°C. The base temperatures in the heated regions oscillated precisely with the period of the imposed power, but the temperature variation was not sinusoidal: the troughs were narrower than the peaks because the heat transport from the base depended on the circulation, particularly lateral flow and convective instability in the boundary layer. The precisely periodic, but non-sinusoidal behavior was further accentuated in the water temperatures, where the cooler periods were again shorter than the warmer periods.

In the boundary layer, there was a large horizontal difference in both temperature and fluctuation amplitude. Temperature oscillations were smallest above the cold boundary and largest over the heated areas. The high frequency fluctuations obvious in the heated parts of the boundary layer correspond to small scale penetrative convection, as seen in previous flow visualizations for steady state forcing (Mullarney *et al.*, 2004). However, the temperature fluctuations were far greater than those measured in the equilibrated steadily-forced cases. These irregular, high frequency (and small scale) temperature fluctuations were similar to those measured during flow adjustment after a new steady forcing was applied (Fig. 2) and which decayed away as the circulation adjusted to the boundary conditions. Note that the temporal average boundary layer temperature measured at 100 mm from the end was cooler than the interior, whereas the warmest temperatures in the boundary layer (seen in the high frequency, small scale events) must be slightly greater than the interior temperature in order to achieve convective heat transport out of the boundary layer and into the plume at the end of the box. Note also the remarkable repetition between forcing cycles, in the detailed temporal behavior of the small-scale convection. In all cases the fluctuations in each half of the box accurately mirrored those in the other half, indicating that the two ends of the box behaved identically.

The temperature records for two very different forcing periods (Fig. 5) show that the flow response was largely similar when time is normalized by the forcing period. Exceptions to this are the amplitudes of the temperature fluctuations, which were larger for longer periods. There was also a slight difference in the shape of the temperature response: the longer forcing period for the imposed fluxes allowed more cooling of the heated base areas during their low power phase. The range of phases of the forcing cycle at which the intermittent penetrative convection signals were measured in the heated boundary layer was insensitive to the forcing period.

In further analysis of the results it is useful to normalize both the time and forcing period by the extensive timescale D^2/κ. (Use of the molecular diffusivity here is not intended to imply that vertical diffusion of heat in the interior of the flow is solely molecular: the addition of dye tracer to the flow revealed a significant amount of eddying and mixing in the interior.) All temperatures are referenced to the fixed cold base temperature θ_C and the

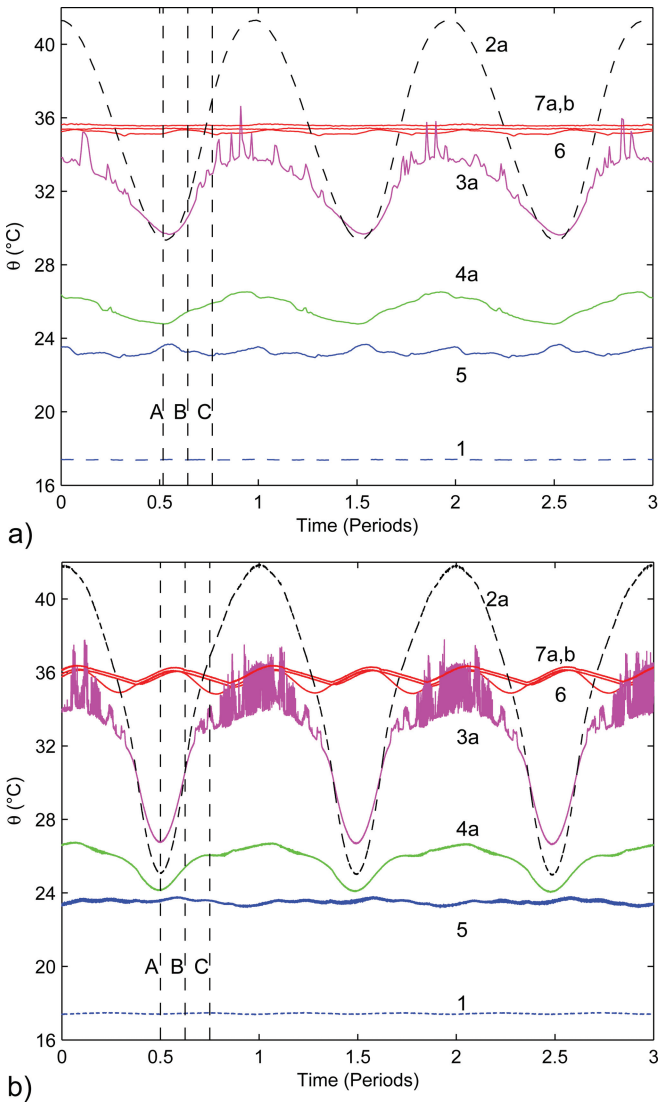

Figure 5. Temperature records for two runs with oscillatory forcing having the same amplitude of applied boundary flux but different periods, plotted against time normalized by the relevant forcing period: (a) run 6, $T_0 = 0.349$ hrs; (b) run 7, $T_0 = 18.9$ hrs (see Table 1). Exactly three periods are plotted for each run, drawn from much longer records of the large-time stationary states. Line colors and numbers are keyed as in previous figures; broken lines are for the base. Redundant boundary layer data from the left hand end are again omitted for legibility. The interior record (red) having the smallest average temperature and largest fluctuation is from just above the boundary layer at the mid-point of the box (thermistor 6). The colder boundary layer temperatures (4a, 5) were very sensitive to the heights of the thermistors above the base, which for these two runs were not the same as in Figure 4. Also indicated are the times (A,B,C) of the three sketches in Figure 3.

difference is normalized by the reference horizontal boundary difference (3). The heating base temperature θ_H, expressed as the normalized horizontal difference $(\theta_H - \theta_C)/\Delta\theta$, oscillated due to the oscillatory power input to the heating regions, and the magnitude of the fluctuations increased with forcing period: its maximum and minimum values are plotted in Figure 6a. The minimum, θ_{Hmin} varied the most and trended toward the reference cold base temperature for large T_0. The peak value, θ_{Hmax}, of the heated boundary temperature, on the other hand, trended toward the result for steady asymmetric forcing (which generates a single plume; horizontal broken line in Fig. 6a), although it remained approximately 2% smaller than that limit at the largest periods used. (Note that the limit $(\theta_{Hmax} - \theta_C)/\Delta\theta = 1.1$ rather than 1.0 owing to the different distribution of basal heating and cooling in the present experiments compared with that used by Mullarney *et al.* (2004) and from which the constant in (3) was derived.) Also indicated in Figure 6a are the results for forcing oscillations having small amplitude: these give relatively small variations in the boundary temperature about that measured for steady symmetric forcing (shown by the solid horizontal line).

An average interior water temperature, $\theta(t)$, was calculated from the three measurement locations in the interior, and the maximum ($\theta_{\max}$) and minimum ($\theta_{\min}$) values found. When referenced to θ_C and normalized (Fig. 6b), this interior temperature serves as a measure of the vertical temperature difference relative to the reference horizontal difference. For small T_0 the interior temperatures increased with forcing period: at $T_0 \to 0$ the finite conductivity of the base and boundary layer water will constrain the flow to the case of steady, symmetric forcing (lower horizontal line in Fig. 6b). For large forcing periods the interior fluctuations were larger: $\theta_{\max}$ increased slowly toward the interior temperature of the steady, asymmetric forcing case (broken horizontal line), whereas $\theta_{\min}$ decreased toward the lower limit, the temperature for steady, symmetric forcing. (The theoretical behavior at very large T_0 is discussed in Section 4.) Between these extrema the time-averaged interior temperature, $\bar{\theta}$, was independent of oscillation period over most of the experimental range: $(\bar{\theta} - \theta_C)/\Delta\theta \approx 0.80 \pm .01$, or 93% of the upper limit given by steady, asymmetric forcing. These results for $a = 1$ show that the vertical temperature difference was approximately 75% of the maximum measured (rather then reference) horizontal difference in the base. For small forcing amplitudes the normalized interior temperature was close to the smaller value (0.67) for steady, symmetric forcing, and the ratio of vertical and (measured) horizontal temperature differences approached the limit of 0.85.

Subtracting the interior and boundary temperatures from each other gives the temperature difference between the heated boundary layer and the interior: the normalized difference between the respective maximum values in each forcing cycle is plotted in Figure 6c. This corresponds to the excess temperature that provides the buoyancy driving the deep convection plume in its strongest phase. For large forcing amplitude ($a = 1$) this excess is $24.5 \pm 0.5\%$ of $\Delta\theta$, independent of forcing period. Allowing for maximum boundary temperatures 4-6% smaller than for steady, asymmetric forcing (see horizontal broken line in Fig. 6a), the result for the excess temperature difference is very close to that in the steady

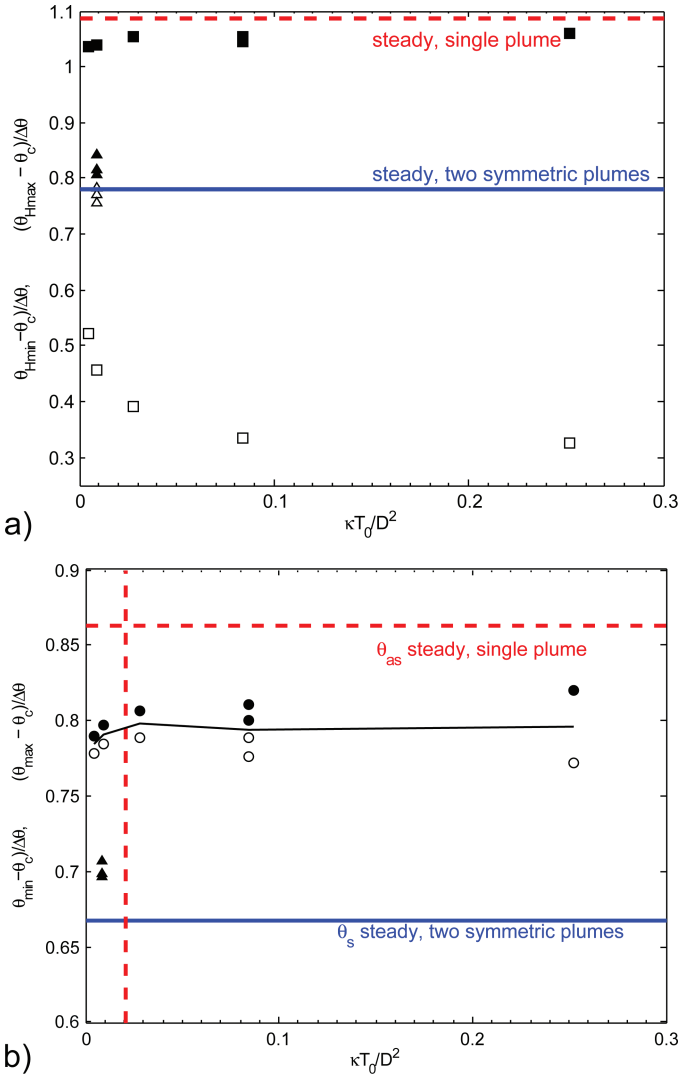

Figure 6. Temperature differences normalized by the reference $\Delta\theta$ (Eq. 3), as functions of the normalized oscillation period: (a) horizontal temperature differences between the heated and cooled areas of the base for a =1 - maximum (filled squares) and minimum (open squares); (b) interior temperatures relative to the cold boundary - peak (filled circle), trough (open circle), mean (black line); (c) excess of the maximum boundary temperature above the peak interior temperature, a difference important to driving the plumes. Corresponding results for runs with smaller oscillation amplitudes a = 0.05, 0.1, 0.2 are also shown - maximum (filled triangles) and minimum (open triangles) values shown in (a), only maximum values shown in (b) for legibility. Corresponding values for steady forcing are shown as horizontal lines not related to the horizontal axis: red line - asymmetric $H_1 = 280\,\mathrm{W}$, $H_2 = 0$; blue line - symmetric $H_1 = H_2 = 140\,\mathrm{W}$. In (b) these are the dimensionless values of θ_{as} and θ_s, respectively. The vertical broken vertical line in (b) indicates the box recycling timescale (Eq. 5). The ratio of the forcing period to the recycling time is also shown on a separate horizontal scale.

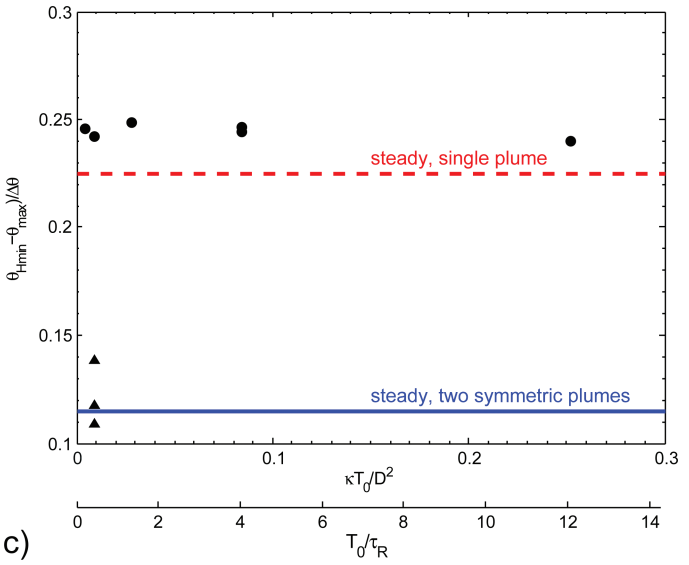

Figure 6. (continued)

case ($22.3 \pm 1\%$). Of course, for small forcing amplitudes the excess instead approaches the value for symmetric steady forcing ($11.4 \pm 1\%$).

The dependence on forcing amplitude was examined using the cases $a = 0$, 0.05, 0.1, 0.2 and 1 for the fixed oscillation period $T_o = 1$ hour (Table 1). The resulting temperatures are plotted as a function of amplitude in Figure 7 and the behavior was straightforward: the normalized interior temperature maximum $\theta_{\max}$ (or equivalently, the vertical temperature difference) simply increased approximately linearly from its value with steady symmetric forcing at $a = 0$ to that at $a = 1$. The excess temperature difference between the interior and the heated boundary maxima (the difference between the red and black lines) also increased linearly. Steadily forced cases with corresponding degrees of asymmetry in the forcing, as reported by Coman *et al.* (2010), gave a consistent behavior with interior temperatures (θ_{steady}) just slightly larger than for the oscillatory cases. This comparison recognizes that the oscillation amplitude a is the maximum forcing asymmetry, which is effectively the normalized difference $R_Q = (H_2 - H_1)/(H_2 + H_1)$ between the heat fluxes to the two heated regions in steady cases.

4. Discussion

The results have been presented above in terms of two external timescales: the time for molecular diffusion through the depth and the imposed oscillation period. Physical understanding of the observed dependence of the flow on the oscillation period also requires consideration of an internal timescale of response. We propose that the response time, τ_R, is that for the volume of the domain to pass through the thermal boundary layer. As the

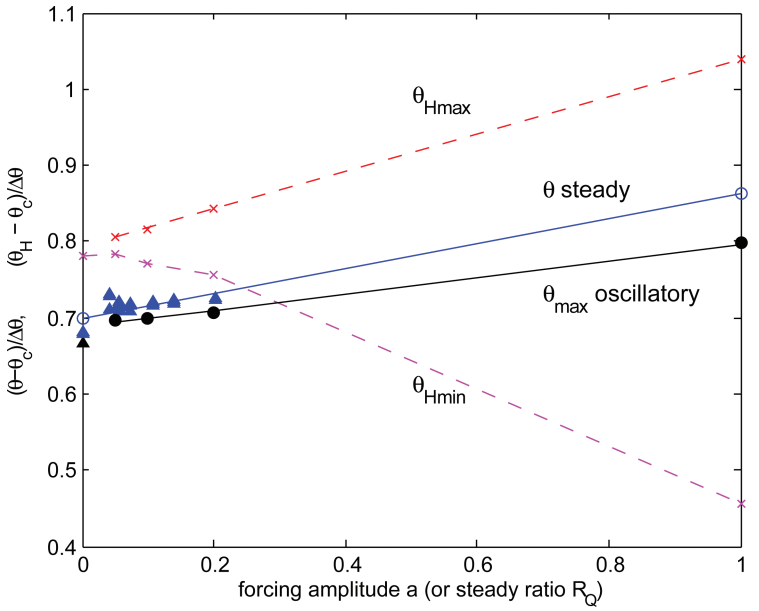

Figure 7. Temperature differences relative to the cold boundary temperature, normalized by $\Delta\theta$, as functions of the oscillation amplitude a (see Eq. 1) at a fixed oscillation period $T_0 = 0.667$ hrs and $\kappa T_0/D^2 = 9 \times 10^{-3}$. Larger solid black circles show the dimensionless $\theta_{\max}$ for the oscillatory cases. The heating boundary temperatures - maximum (θ_{Hmax}) and minimum (θ_{Hmin}) in the oscillation cycle - are plotted as red and magenta crosses (trends shown by red and magenta dashed lines), respectively. The corresponding quantities from a run with steady symmetric forcing are plotted at $a = 0$. The interior temperatures (θ steady) for previous experiments with steady forcing (Coman *et al.*, 2010) are plotted for comparison (blue triangles and circle, blue line): for these cases the amplitude a is approximately equivalent to the steady asymmetry in the heating ratio R_Q.

water passes through the boundary layer, its temperature is altered. The flow may remain close to equilibrium with its instantaneous boundary conditions if the oscillation period is very much greater than the recycling time, whereas it will not have time to respond to boundary fluctuations on timescales much shorter than τ_R. The response timescale is longer then the time for the plume outflow to fill the volume of the domain (in the experiments τ_R was approximately 5 times longer), as the plume transport includes substantial recycling of interior water by entrainment and entrainment is not effective in changing the interior temperature in line with changes in the thermal boundary conditions.

The response timescale for the experimental configuration can be found by considering a steady state circulation and the convection solution of Hughes *et al.* (2007). For that solution a Munk-like advection-diffusion balance in the interior of the box (everywhere outside an end-wall plume) is coupled with a turbulent plume solution. The solution, including the resulting thermal boundary layer, is inviscid. However, it gives a boundary layer thickness

and Nusselt-Rayleigh number relation in agreement those from an earlier viscous boundary layer analysis (Rossby, 1965) and experimental results (Mullarney *et al.*, 2004). The vertical volume flux (per unit width) into the thermal boundary layer is given by

$$W_e L = 1.83 E^{1/3} (Pr Ra_F)^{1/6} \kappa^*, \tag{4}$$

where E $(= 0.1)$ is the entrainment constant for the plume, W_e is the vertical velocity at the edge of the boundary layer and κ^* is the effective diffusivity. The recycling, or 'box filling', timescale is then $\tau_R = LD/W_e L$. In dimensionless form:

$$\kappa^* \tau_R / D^2 = 0.546 (L/D)(E^2 Pr Ra_F)^{-1/6}. \tag{5}$$

If κ^* under the experimental conditions is assumed equal to the molecular diffusivity κ, and we assume a single full-strength plume, the adjustment times in all of the experiments are $\tau_R = (5.58 - 5.69) \times 10^3$ s. The use of κ for the non-dimensionalization is not true to the theoretical solution and it cannot generally be assumed to be a close approximation to the effective κ^*. Under laboratory conditions similar to these experiments κ^* has been estimated to be 2–3 times greater than the molecular value for heat - as a consequence of mixing driven by the convective circulation (Hughes *et al.*, 2007) - and will be a function of the governing parameters. In the oceans, the effective vertical diffusivity is much greater owing to other energy sources and processes generating small-scale mixing. However, we are unable to predict κ^* and κ presents an alternative, clearly defined extensive variable. The normalized value of this timescale for the experiments (indicated by a vertical line in Fig. 6b) is $\kappa \tau_R / D^2 \approx 0.021$. The ratio of the imposed forcing periods to the recycling timescale τ_R is shown in Figure 6.

The measured adjustment to new steady boundary conditions, shown in Figure 2, required approximately $(3 - 4)\tau_R$. The diffusion timescale is 50 times greater than τ_R and therefore plays no significant role in adjustment - and we do not need to be concerned with the value of κ or κ^* used in non-dimensionalizing. The longest oscillatory forcing periods used were over 20 times the flow recycling timescale. However, within each forcing cycle the boundary conditions changed from, for example, symmetric to the maximum asymmetry in one quarter of a period, equivalent to just five recycling times. Hence it is not surprising that the longest period did not represent quasi-equilibrium, a state in which the interior temperature is expected to fluctuate between the symmetric and asymmetric forcing limits in Figure 6b.

The interior temperature fluctuations (Fig. 6) are produced by the varying strength of the stronger plume: when a plume passes through its strongest phase (ie. greatest heat transport), θ passes through its maximum, $\theta_{\max}$. As there are two plumes, this occurs twice per cycle. The interior minimum $\theta_{\min}$ corresponds to the symmetric phase of two equal plumes (again twice per cycle), and not to the weakest phase of a plume. The boundary conditions also change most rapidly at the two symmetric phases and most slowly at the most asymmetric

phases. The heat supplied to the interior by the strongest plume is a rectified sinusoidal function of time, and the interior temperature (Fig. 5) also looks somewhat like a rectified oscillation, with sharp troughs and rounded peaks. For very long forcing periods the peak interior temperature will coincide with the interior temperature, θ_{as}, measured in the steady runs having all of the heat transported through one plume; the minimum will coincide with the interior temperature, θ_s, in the steady runs having two equal plumes (the two limits shown in Fig. 6). The time average for large T_0 will be $\bar{\theta} = \theta_s + (2/\pi)(\theta_{as} - \theta_s)$, which gives

$$(\bar{\theta} - \theta_C)/\Delta\theta = 0.79 \tag{6}$$

and is identical to the average of the maxima and minima plotted in Figure 6. The same process makes the time average independent of forcing period, while the amplitude of the interior fluctuations becomes small for periods less than τ_R.

5. Implications for the oceans

The experiments reveal potentially important aspects of ocean circulation under fluctuating surface heat fluxes. The ocean response timescale τ_R, the time for the total ocean volume to be cycled through the thermocline and sinking regions, is approximately 4000 years (calculated from an average depth 3780 m, an area 3.6×10^{14} m^2 and an estimated 10 ± 5 Sv of sinking through the base of the thermocline, noting that the global production of around 30 Sv of deep and bottom water includes a dilution, by a factor of 2 to 3, of dense water by entrainment at depths below 700 m; see Hughes and Griffiths (2006) for a discussion of relevant measurements). For comparison, ocean measurements imply an average diffusivity $\kappa^* \sim 10^{-5} - 10^{-4}$ m^{2}s^{-1} and a diffusion timescale $D^2/\kappa^* \sim 5000 - 50,000$ years, and we have argued that this process is not important to the flow adjustment.

The annual 'see-saw' of forcing between northern and southern hemispheres therefore has such a high frequency ($T_0/\tau_R \sim 2 \times 10^{-4}$) that it cannot cause bulk temperature fluctuations in the abyssal ocean. On the other hand, the seasonal cycle can have a significant influence on the average abyssal temperature. The annual mean state, if the seasonal forcing amplitude were $a = 1$, is predicted by adapting (6) to forcing at the upper surface: $\bar{\theta} = \theta_H - 0.79\Delta\theta$, where the reference temperature in the stabilising region is now the highest (tropical) surface temperature θ_H. Given $\theta_H \approx 28$°C and the overall meridional surface difference $\Delta\theta \approx 30$°C, the predicted time-averaged interior temperature $\bar{\theta} \approx 4.3$°C. The lowest possible interior (potential) temperature, given the present day surface temperatures, is estimated by supposing the surface buoyancy inputs were constrained to be steady with the same total cooling flux, but all in one hemisphere. In that case sinking would occur in only one hemisphere and the interior temperature would be given by $\theta = \theta_H - 0.86\Delta\theta \approx 2.2$°C. In contrast, if the buoyancy forcing were steady and symmetric (the limit $a \to 0$), the highest predicted interior temperature $\theta \approx 7.9$°C. Thus both the distribution and the oscillatory

nature of seasonal forcing have significant influences. It is likely that a somewhat smaller forcing amplitude $a < 1$ is appropriate for the annual 'see-saw', because sea surface cooling does not vanish in summer at high latitudes. Despite the very high frequency of the annual cycle, this implies a time average somewhere in the range $4.3 \leq \bar{\theta} \leq 7.9°C$, assuming a symmetric oscillation. The abyssal waters will be warmer for smaller seasonal forcing amplitudes. However, we point out below that these values are not expected to match the present potential temperature of the deep oceans (an average 3°C below a depth of 1000 m), as the oceans may remain significantly colder because the last glacial maximum was a mere 19 Ka ago.

There is a range of much slower fluctuations in the climate system. Millennial oscillations, such as the warm events punctuating the glacial climate prior to 20 Ma ago and detected in the northern hemisphere climate record (Dansgaard-Oeschger cycles, Dansgaard *et al.* (1993)), have a period so short that according to our results, they will not have produced significant fluctuations of the deep ocean temperature. The Milankovitch or glacial cycles have three dominant periods: 23,000, 41,000 and 100,000 years (Berger and Loutre, 1991; Petit *et al.*, 1999; Augustin *et al.*, 2004; Zachos *et al.*, 2001), corresponding to $T_0/\tau_R \approx 6$, 10 and 25. An extrapolation of the experimental results implies that even the longest of these cycles is too rapid to allow the properties in the abyssal ocean depths to remain close to equilibrium with the changing surface conditions. Although the longest of the Milankovitch cycles (due to changes in the eccentricity of the earth's orbit) is not characterized by a constant total heat input as in our experiments, our results serve to emphasize the extremely long timescales required for the ocean stratification to adjust to changing inputs. On the other hand, the glacial cycles are long enough to produce a substantial fluctuation in abyssal ocean temperatures. This raises the possibility of a continuing slow climate 'drift' today resulting from past climate changes. Such a drift will be slow and insignificant compared to the pace of recent observed climate changes, but the difference between the measured and equilibrium abyssal temperatures could be significant. It also suggests that realistic high-resolution global ocean and climate simulations may require extremely long times to 'spin up' (Treguier *et al.*, 2010) and adjust to a stationary state or to imposed boundary conditions.

Our aim here has been to draw out the dependence of the abyssal ocean temperature and the overall stratification on climate oscillations using a simple convective model. The focus is on the deep sinking process, which is not resolved in climate models. Quantitative extrapolation of the results to the oceans must of course be tempered by the roles of factors not considered here. These include topographic sills and slopes, wind-driven vertical pumping (particularly Southern Ocean upwelling), planetary rotation (particularly in geostrophic slope plumes; Hughes and Griffiths (2006)), the nature of the thermal boundary conditions (here a mixture of applied temperature and applied heat flux; Tziperman *et al.* (1994)), buffering of surface ocean temperatures by freezing, modification of the buoyancy of dense water by thermobaricity and cabbeling, and the uncertain global distribution of past climate fluctuations.

6. Conclusions

The experiments demonstrate that convective overturning forced by oscillatory boundary conditions is qualitatively different from the circulation with steady forcing. Whereas steady forcing leads to a delicate balance of the flow and temperature field, and achieves zero net buoyancy flux through every level, time-varying forcing involves periods of imbalance, much stronger overturning and more vigorous small-scale convection in the regions of destabilising buoyancy flux. Horizontal intrusions occur at depths near the edge of the thermal boundary layer, driven by the plumes in their weaker phases (MacCready *et al.*, 1999), and tracer from the surface is more effectively distributed throughout the interior. Although the present experiments focused on cases with constant total heat input and equal time-averaged heat input at the two destabilizing regions, these observations will hold for oscillatory forcing more generally, including systems having a single sinking region. The same qualitative features were observed across the whole range of forcing periods used in the laboratory.

The stratification under oscillatory forcing differs from that produced by applying the same total heat input as steady boundary conditions: the stratification is greater than that given by symmetric forcing and two equal plumes, and less than that given by forcing the same total heat transport through a single plume. Thus the result for an oscillating turbulent plume and the 'filling-box' stratification driven by a net buoyancy input (Killworth and Turner, 1982), where the stratification is set by the strongest phase of the plume, does not carry over to the case having zero net time-averaged buoyancy input. The time-averaged stratification is insensitive to the forcing period, but the amplitude of fluctuations in the interior temperature increases with both forcing amplitude and period. For forcing periods less than the internal volume recycling time τ_R, the interior temperature variability is very small, whereas for forcing periods $T_0 > 10^2\tau_R$ the interior temperature fluctuates between the values for steady, symmetric forcing and steady, asymmetric forcing.

For the oceans the results of this simple convective model imply that climate fluctuations having timescales of millennia or less are too rapid to produced significant fluctuations of the deep ocean temperature. The distribution of surface forcing and fluctuation amplitude can, however, influence the mean state, a conclusion that applies even for the annual seasonal 'see-saw' between hemispheres. For example, the abyssal waters will be warmer for smaller seasonal forcing amplitudes. Climate fluctuations having the much longer timescales of the glacial cycles, on the other hand, will produce substantial fluctuations in abyssal temperatures, although even the longest of these (at a period $T_0/\tau_R \approx 25$) is too rapid for the deep ocean to remain close to equilibrium with the changing surface conditions. Thus extremely long timescales are required for the adjustment of ocean stratification. We should not expect the present ocean to be in equilibrium with the present climate and realistic climate simulations may require extremely long 'spin-up' times.

Acknowledgments. We thank Tony Beasley for assistance with the laboratory experiments. The work was partly funded by the Australian Research Council (DP1094542). RWG enjoyed stimulating

and formative collaboration with Melvin Stern on instabilities of ocean currents, beginning at the 1980 WHOI Geophysical Fluid Dynamics summer program.

REFERENCES

Augustin, L. *et al.* 2004. Eight glacial cycles from an Antarctic ice core. Nature, *429*, 623–628.

Beardsley, R. C. and J. F. Festa. 1972. A numerical model of convection driven by a surface stress and non-uniform heating. J. Phys. Oceanogr., *2*, 444–455.

Berger, A. and M. F. Loutre. 1991. Insolation values for the climate of the last 10 million years. Quatern. Sci. Rev., *10*, 297–317.

Bryan, F. 1987. Parameter sensitivity of primitive equation ocean general circulation models. J. Phys. Oceanogr., *17*, 970–985.

Colin de Verdière, A. 1988. Buoyancy driven planetary flows. J. Mar. Res., *46*, 215–265.

Coman, M. A., R. W. Griffiths, and G. O. Hughes. 2010. The sensitivity of convection from a horizontal boundary to the distribution of heating. J. Fluid Mech., *647*, 71–90.

Dansgaard, W., S. J. Johnsen, H. B. Clausen, D. Dahljensen, N. S. Gundestrup, C. U. Hammer, C. S. Hvidberg, J. P. Steffensen, A. E. Sveinbjornsdottir, J. Jouzel, and G. Bond. 1993. Evidence for general instability of past climate from a 250-Kyr ice-core record. Nature, *364*, 218–220.

Hignett, P., A. Ibbetson, and P. D. Killworth. 1981. On rotating thermal convection driven by non-uniform heating from below. J. Fluid Mech., *109*, 161–187.

Hughes, G. O. and R. W. Griffiths. 2006. A simple convective model of the global overturning circulation, including effects of entrainment into sinking regions. Ocean Model., *12*, 46–79.

—— 2008. Horizontal convection. Annu. Rev. Fluid Mech., *40*, 185–208.

Hughes, G. O., R. W. Griffiths, J. C. Mullarney, and W. H. Peterson. 2007. A theoretical model for horizontal convection at high Rayleigh number. J. Fluid Mech., *581*, 251–276.

Killworth, P. D. and J. S. Turner. 1982. Plumes with time-varying buoyancy in a confined region. Geophys. Astrophys. Fluid Dyn., *20*, 265–291.

MacCready, P., W. E. Johns, C. G. Rooth, D. M. Fratantoni, and R. A. Watlington. 1999. Overflow into the deep Caribbean: effects of plume variability. J. Geophys. Res., *104*, 25913–25935.

Manabe, S. and R. J. Stouffer. 1995. Simulation of abrupt climate-change induced by fresh-water input to the North Atlantic Ocean. Nature, *378*, 165–167.

Mullarney, J. C., R. W. Griffiths, and G. O. Hughes. 2004. Convection driven by differential heating at a horizontal boundary. J. Fluid Mech., *516*, 181–209.

—— 2006. The effects of geothermal heating on the ocean overturning circulation. Geophys. Res. Lett., *33*, L02607, doi:10.1029/2005GL024956.

Munk, W. H. 1966. Abyssal recipes. Deep-Sea Res., *13*, 707–730.

Paparella, F. and W. R. Young. 2002. Horizontal convection is non-turbulent. J. Fluid Mech., *466*, 205–214.

Park, Y. and K. Bryan. 2001. Comparison of thermally driven circulation from a depth-coordinate model and an isopycnal model. Part II: The difference and structure of the circulations. J. Phys. Oceanogr., *31*, 2612–2624.

Petit, J. R., J. Jouzel, D. Raynaud, N. I. Barkov, J. M. Barnola, I. Basile, M. Bender, J. Chappellaz, J. Davis, G. Delaygue, M. Delmotte, V. M. Kotlyakov, M. Legrand, V. Lipenkov, C. Lorius, L. Pèpin, C. Ritz, E. Saltzman, and M. Stievenard. 1999. Climate and atmospheric history of the past 420,000 years from the Vostok ice core. Nature, *399*, 429–436.

Rahmstorf, S. 1996. On the freshwater forcing and transport of the Atlantic thermohaline circulation. Climate Dyn., *12*, 799–811.

Rossby, H. T. 1965. On thermal convection driven by non-uniform heating from below: an experimental study. Deep-Sea Res., *12*, 9–16.

—— 1998. Numerical experiments with a fluid non-uniformly heated from below. Tellus, *50*, 242–257.

Suginohara, N. and S. Aoki. 1991. Buoyancy-driven circulation as horizontal convection on beta-plane. J. Mar. Res., *49*, 295–320.

Treguier, A. M., J. L. Sommer, J. M. Molines, and B. de Cuevas. 2010. Response of the Southern Ocean to the Southern Annular Mode: Interannual variability and multidecadal trend. J. Phys. Oceanogr., *40*, 1659–1668, doi: 10.1175/2010JPO4364.1.

Tziperman, E., J. R. Toggweiler, Y. Feliks, and K. Bryan. 1994. Instability of the thermohaline circulation with respect to mixed boundary-conditions - Is it really a problem for realistic models? J. Phys. Oceanogr., *24*, 217–232.

Wang, W. and R. X. Huang. 2005. An experimental study on thermal convection driven by horizontal differential heating. J. Fluid Mech., *540*, 49–73.

Wright, D. G. and T. F. Stocker. 1991. A zonally averaged ocean model for the thermohaline circulation. Part I: Model development and flow dynamics. J. Phys. Oceanogr., *21*, 1713–1724.

Zachos, J., M. Pagani, L. Sloan, E. Thomas, and K. Billups. 2001. Trends, rhythms, and aberrations in global climate 65 Ma to present. Science, *292*, 686–693.

Received: *15 April, 2011*; revised: *11 August, 2011*.